Graphabs

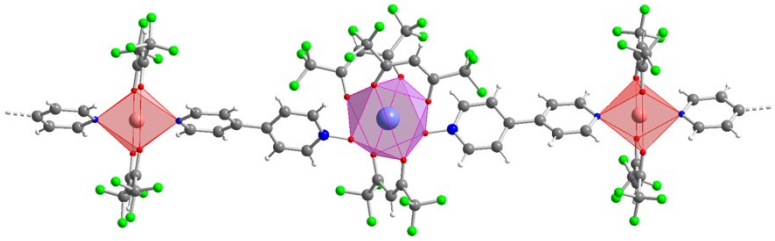

Revised Manuscript

Dalton Transactions

1D hetero-bimetallic regularly alternated 4*f*-3*d* coordination polymers based on *N*-oxide-4,4'-bipyridine (bipyMO) as linker: photoluminescent and magnetic properties

Lidia Armelao,[§†] Daniela Belli Dell'Amico,[‡] Gregorio Bottaro,[§†] Luca Bellucci,[§] Luca Labella,[‡*] Fabio Marchetti,[‡] Carlo Andrea Mattei,[‡] Federica Mian,[§†] Francesco Pineider,[‡] Giordano Poneti[#] and Simona Samaritani[‡]

[§]*Dipartimento di Scienze Chimiche, Università di Padova, via Marzolo 1,I-35131*

[†]*CNR ICMATE and INSTM, Dipartimento di Scienze Chimiche, Università di Padova, via Marzolo 1,I-35131*

[‡]*Dipartimento di Chimica e Chimica Industriale and CIRCC, Università di Pisa, via Giuseppe Moruzzi 13, I-56124*

[#]*Instituto de Química, Universidade Federal do Rio de Janeiro, Avenida Athos da Silveira Ramos, 149, Centro de Tecnologia – Cidade Universitária,21941-909, Rio de Janeiro, Brazil*

ABSTRACT

The heterotopic divergent ligand *N*-oxide-4,4'-bipyridine (bipyMO) has been herein exploited for the preparation of hetero-bimetallic coordination polymers where $Ln(hfac)_3$ and $M(hfac)_2$ nodes regularly alternate (Hhfac=1,1,1,5,5,5-hexafluoro-2,4-pentanedione), bipyMO being able to selectively use its two potential coordination sites to discriminate the metal ions. The synthesis of three coordination polymers, $[Ln(hfac)_3M(hfac)_2(bipyMO)_2]_n$ (Ln=Eu, M=Zn, **1**; Ln=Eu, M=Cu, **2**, Ln=Dy, M=Co, **3**), was carried out by reacting the appropriate $[M(hfac)_2(bipyMO)]_n$ and $[Ln(hfac)_3]$ precursors in toluene in the presence of the stoichiometric amount of bipyMO. The products were characterized by elemental analysis, X-Ray powder diffraction, and FTIR spectroscopy. Single crystal X-ray diffraction studies carried out on **2** showed that it was formed by chains containing the hexa-coordinated 3*d* metal ($Cu(hfac)_2[N]_2$) and the octa-coordinated lanthanide ($Eu(hfac)_3[O]_2$) nodes, where [N] and [O] stand for the donor atom of the bridging divergent ligand. The X-Ray powder diffraction patterns of the three compounds and the comparison of their cell constant values allowed to establish that the derivatives were isotypic. Photoluminescence (PL) studies on microcrystalline sample powders evidenced a bright red emission for **1** with absolute PL quantum yield of 0.24. The sensitized emission of Eu^{3+} can be excited in a wide wavelength range, from UV to visible, up to ≈ 450 nm. Conversely, europium emissions are not detectable in **2** due to the presence of $Cu(hfac)_2(bipyMO)$ moieties whose strong absorptions overlap Eu^{3+} transitions.

Magnetic measurements conducted on **3** revealed the presence of a weak ferromagnetic interaction below 2.1 K. An ac susceptibility study highlighted a slow relaxation of the magnetization of **3** with an applied static magnetic field of 0.1 T, which could be equally fitted with a Orbach-direct or a Raman-direct mechanism. No relaxation dynamics were detected without the application of a static magnetic field.

Introduction

The synthesis of heterometallic coordination polymers (CPs) involving 3*d* and 4*f* metal ions is increasingly receiving great attention for the potential applications of such systems as functional materials in magnetism, molecular adsorption, luminescence, catalysis and chemical separation.[1] Several examples are reported in the literature,[2] the recurring building blocks being: (a) bis(oxamato)M(II) complexes; (b) tris(oxalato) complexes; (c) polycyano complexes; (d) $[M(bpca)_2]$ [Hbpca = bis(2-pyridylcarbonyl) amine]. Recent reports showed the possibility to self-assemble *4f-3d* heterometallic molecular chains by exploiting the different binding features of N, O-donating organic radicals belonging to the nitronyl-nitroxide[3] and to the verdazyl[4] classes. The simple neutral heterotopic *N*-oxide-4,4'-bipyridine (Scheme 1) has been rarely used to synthesize CPs, at variance with the abundant coordination chemistry of the homotopic 4,4'-bipyridine (bipy)[5] and 4,4'-bipyridine-*N,N'*-dioxide (bipyDO).[6] In the few examples reported in the literature, bipyMO acts as a connector between two metal centres with formation of homo-metallic coordination polymers[7], or it coordinates in a hypo-dentate mode[8], being N- or O- linked in dependence of the metal ion identity. In the latter case the uncoordinated site (O or N, respectively), in the presence of water or other protic species, can be engaged in hydrogen bonding with formation of 2D and 3D networks.

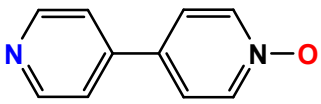

Scheme 1 *N*-oxide-4,4'-bipyridine (bipyMO)

It is interesting to report that among the known homo-metallic bipyMO-based CPs [metal ions Pb(II),[7a,d] Bi(III)[7c]], a recurring motif is the formation of alternated moieties $M^*[O]_2$ and $M^*[N]_2$, where [N] and [O] specify the donor atom of the bridging bipyMO and M* indicates the metal ion with its complementary coordination sphere.

Recently, some of us have prepared and structurally characterized four isotypic homo-metallic coordination polymers of 3d metals, $[M(hfac)_2(bipyMO)]_n$ (M = Zn, Cu, Co, Mn; hfac =

hexafluoroacetylacetonate).[9] Also in these monodimensional CPs two different metal coordination polyhedra $M(hfac)_2[N]_2$ and $M(hfac)_2[O]_2$ alternate, suggesting that this arrangement is favoured with respect to a continuous sequence of $M(hfac)_2[O][N]$ moieties. The simple consideration that bipyMO could discriminate between two metal centres showing a different affinity for nitrogen and oxygen donor ligands, drove us to the synthesis of the hetero-bimetallic CP $[Cu(hfac)_2Mn(hfac)_2(bipyMO)_2]_n$ containing ordered sequences of $Cu(hfac)_2[N]_2$ and $Mn(hfac)_2[O]_2$ moieties, that was obtained by a self-rearrangement of the two homo-metallic CPs in 1:1 molar ratio carried out in MeCN.[9]

On the basis of this outcome we considered that bipyMO could be an excellent connector between a lanthanide(III) and a *d* block metal, acting as an O-donor to the lanthanide and a N-donor to the *d*-metal. Nevertheless, the self-assembly of a hetero-metallic CP is often a challenge, especially when lanthanide ions are involved, since these metal centres are characterized by a remarkable lability as well as by a considerable flexibility in both coordination number and geometry.[10]

To avoid inter-exchange of the spectator ligands coordinated to the different metal centres, hexafluoroacetylacetonato anions were used for both M and Ln. Moreover, the choice of the nodes $M(hfac)_2$ and $Ln(hfac)_3$ appeared proper for the occupancy of four and six coordination sites by the chelating anionic hfac ligands in the M (usually hexacoordinated) and Ln (often octacoordinated) coordination spheres, respectively, so leaving two available free positions on both centres. In addition, the $[Ln(hfac)_3(H_2O)_2]$ (Ln = Eu, Dy) precursors can be easily prepared, have good solubility in organic solvents and show a pronounced Lewis acid character of the metal centre due to the electron-withdrawing effect of the β-diketonato CF_3 substituents.

This strategy drove with success to the synthesis of three 4*f*-3*d* hetero-metallic coordination polymers that are here reported. The choice of the lanthanide metal centres (Eu, Dy) was based on the interest towards the photoluminescence properties of europium and the peculiar magnetic features of dysprosium.

From the magnetic point of view, lanthanide ions play a starring role. Their high magnetic moment, arising from spin as well as from unquenched orbital moment, is responsible for the highest single-ion magnetic anisotropies found in the periodic table.[11] As such, double-decker complexes were among the first molecular species exhibiting slow relaxation of their magnetization without the presence of magnetically coupled ions in a molecular complex.[12] Aiming to increase the energy barrier for the magnetic relaxation, the magnetic behaviour of more complex structures has been investigated as well, especially 4f-4f,[13] 3d-4f [14] and 2p-4f coupled systems.[15] The dynamics of the magnetization of lanthanide-based clusters depend on the electronic structure of the ions as well, on the structure of the first coordination sphere and on magnetic interactions in the solid state, and

significant research efforts are aimed at determining magneto-structural correlations in lanthanide-based Single Molecule Magnets.[16] Of particular interest is the role of an exchange interaction between magnetic ions on the dynamics of their magnetic moment. While some reports show that a weak magnetic coupling in the solid state may cause a bias effect on the relaxing ions, actually slowing their magnetization dynamics,[17] additional evidence exists of a decrease of the magnetic relaxation time in exchange coupled 3*d*-4*f* clusters.[18] Here we report the dynamics of the magnetization of a 3*d*-4*f* system showing a very weak ferromagnetic coupling in the solid state.

Experimental

General Information

All manipulations were performed under a nitrogen atmosphere, unless otherwise stated. FTIR spectra were recorded with a Perkin–Elmer ‘‘Spectrum One’’ spectrometer, equipped with an ATR accessory. Elemental analyses (C, H, N) were performed at Dipartimento di Scienze e Tecnologie Chimiche, Università di Udine. $[M(hfac)_2(bipyMO)]_n$ (M = Zn, Cu, Co),[9] $[Eu(hfac)_3(H_2O)_2]$ and $[Dy(hfac)_3(H_2O)_2]$ were prepared according to the literature.[19] Commercial toluene (Sigma Aldrich) and methanol (Aldrich) were used as received.

Synthesis

The synthesis of **1** is reported in detail. Analogous procedure was followed for the synthesis of **2** and **3**.

$[Eu(hfac)_3Zn(hfac)_2(bipyMO)_2]_n$, 1- To a suspension of $[Zn(hfac)_2(bipyMO)]_n$ (0.39 g, 0.60 mmol) in toluene (25 mL) $bipyMO\cdot 2H_2O$ (0.14 g, 0.67 mmol) was added. After refluxing for 1 h, a solution of $[Eu(hfac)_3(H_2O)_2]$ (0.53 g, 0.65 mmol) in toluene (70 mL) was added to the mixture at room temperature. The system was refluxed for 3 h and then cooled to room temperature. The suspension was filtered and the colorless solid was dried under vacuum (780 mg, 81.4 % yield as $[Eu(hfac)_3Zn(hfac)_2(bipyMO)_2]_n$. Anal. Calcd for $C_{45}H_{21}EuF_{30}N_4O_{14}Zn$: C, 33.8; H, 1.3; N, 3.5 %. Found: C, 34.0; H, 1.0; N: 3.5 %. FTIR-ATR: (1700-700 cm^{-1} range) 1644s, 1615w, 1605m, 1572w, 1557m, 1543w, 1531m, 1516w, 1495m, 1482s, 1415m, 1344w, 1324w, 1317w, 1251s, 1225s, 1197s, 1184s, 1139s, 1109s, 1110m, 1089s, 1040m, 1015w, 944w, 861m, 853m, 821m, 800s, 770w, 741m, 714w cm^{-1}. The product was soluble in methanol and ethanol at room temperature. By slow evaporation of a methanol solution, single crystals suitable to check the unit cell through X-ray diffractometric studies were obtained: *a* 13.4371(6); *b* 13.9893(6); *c* 17.0772(7) Å; α 81.309(2); β 74.349(2); γ 66.031(2)°.

$[Eu(hfac)_3Cu(hfac)_2(bipyMO)_2]_n$, 2- 74.3 % yield as $[Eu(hfac)_3Cu(hfac)_2(bipyMO)_2]_n$. Anal. Calcd for $C_{45}H_{21}CuEuF_{30}N_4O_{14}$: C, 33.9; H, 1.3; N, 3.5 %. Found: C, 34.0; H, 1.2; N: 3.5 %. FTIR-ATR: (1700-700 cm^{-1} range) 1645s, 1614m, 1553m, 1531m, 1518w, 1481s, 1417m, 1338w, 1317w, 1251s, 1222s, 1197s, 1185s, 1140s, 1110s, 1101m, 1089m, 1078m, 1041m, 1022w, 943w, 863w, 853m, 823m, 800s, 769w, 741w, 713w cm^{-1}. The product is soluble in methanol and ethanol at room temperature. By slow evaporation of a methanol solution single crystals suitable for X-Ray diffractometric studies were obtained.

$[Dy(hfac)_3Co(hfac)_2(bipyMO)_2]_n$, 3- 80.8 % yield as $[Dy(hfac)_3Co(hfac)_2(bipyMO)_2]_n$. Anal. Calcd for $C_{45}H_{21}CoDyF_{30}N_4O_{14}$: C, 33.7; H, 1.3; N, 3.5 %. Found: C, 34.1; H, 1.2; N: 3.3 %. FTIR-ATR: (1700-700 cm^{-1} range) 1646s, 1639s, 1616w, 1605m, 1557m, 1530m, 1496 (f), 1481 s, 1415 m, 1345w, 1316w, 1251s, 1218s, 1197s, 1184s, 1139s, 1110s, 1091s, 1040m, 1013w, 944w, 861m, 853m, 821m, 799s, 769w, 742m, 714w cm^{-1}. The product is soluble in methanol and ethanol at room temperature. By slow evaporation of a methanol solution, single crystals suitable to check the unit cell through X-ray diffractometric studies were obtained: *a* 13.27(5), *b* 13.80(6), *c* 16.96(6) Å, α 81.70(4), β 75.35(9), γ 66.44(7) °.

Crystallographic analysis

Crystals of **2**, glued at the end of glass fibers, were studied at room temperature by means of a Bruker SMART Breeze CCD diffractometer equipped with graphite monochromated Mo-$K\alpha$ radiation (λ = 0.71073 Å). Indexing was performed using APEX2[20] software. The crystal data are listed in Table 1. Probably due to the disorder of fluorinated groups, the diffraction intensities rapidly reduced to zero at θ angles greater than 30°. Collected intensities were corrected for Lorentz and polarization effects and for absorption by an integration method based on the crystal shape implemented in SADABS program.[21] The structure was solved using SHELXS-2014/7 and refined using SHELXL-2014/7 program packages.[22] Hydrogen atoms were placed in geometrically calculated positions and included in the refinement process using riding model. Significant disorder was observed in several CF_3 groups and one of them was refined as placed in two different positions with geometric restraints fixing to one the total occupancy. The final reliability factors are listed in Table 1. Some routines contained in the WINGX suite[23] were also used. Detailed structural parameter for **2** were deposited with the Cambridge Crystallographic Data Centre, see table 1 for deposition number, and may be obtained free of charge by quoting this paper.

Table 1. Crystal data and refinement summaries

Identification code	2
CCDC number	1586255
Empirical formula	$C_{45}H_{21}F_{30}N_4O_{12}CuEu$
Formula weight	1595.16
Crystal system	Triclinic
Space group	$P\ \bar{1}$
a (Å)	13.5009(8)
b (Å)	13.9971(8)
c (Å)	17.0203(9)
α (°)	80.448(2)
β (°)	73.862(2)
γ (°)	65.595(5)
Volume (Å^3)	2808.8(3)
Z	2
ρ_{calc} (g cm^{-1})	1.886
μ (mm^{-1})	1.647
F(000)	1554
θ range (°)	2.1 to 26.5
Reflections collected	97537
Independent reflections	11621
Goodness-of-fit on F^2	1.088
Final R_1 [$I \geq 2\sigma(I)$]	0.0537

Photoluminescence

Luminescence spectra were recorded on microcrystalline sample powders at room temperature with a Fluorolog-3 (Horiba Jobin Yvon) spectrofluorimeter equipped with a double-grating monochromator in both the excitation and emission sides coupled to a R928P Hamamatsu photo-multiplier, and a 450 W Xe arc lamp as the excitation source. The emission spectra were corrected for detection and optical spectral response of the spectrofluorimeter through a calibration curve supplied by the manufacturer. The excitation spectra were corrected for the spectral distribution of the lamp intensity by using a photodiode reference detector. The luminescence lifetimes in the micro-milli-second time scale were measured by a pulsed Xe lamp with variable repetition rate and elaborated with standard software fitting procedures. The experimental uncertainty on τ values is 10%. Absolute photoluminescence quantum yields were calculated by corrected emission spectra obtained from a Spectralon-coated integrating sphere accessory (4“, F-3018, Horiba Jobin-Yvon) fitted in the fluorimeter sample chamber. Three independent measurements were carried out on each sample with an estimated error of ± 20 %. Quantum yield values are independent of the excitation wavelength in the investigated range.

Magnetometry

Samples used for direct current (dc) and alternating current (ac) magnetic investigations consisted of pellets made out of microcrystalline powders of **3**. Direct current magnetic investigations were

performed using a Quantum Design MPMS instrument equipped with a 5 T magnet. The temperature dependence of the magnetization (M) was followed from 1.8 to 300 K by applying a 1 T field from 300 to 45 K and a 0.1 T field below 45 K to reduce magnetic saturation effects. Magnetic susceptibility per mole (χ_M) was then evaluated as $\chi_M = M_M/B$. Alternating current magnetic susceptibility analysis was performed with a Quantum Design PPMS setup working in the 10 – 10000 Hz range with zero and 0.1 T applied static field. Magnetic data were corrected for the sample holder contribution and for the sample diamagnetism using Pascal's constants.[24] The ac susceptibility data were analysed within the extended Debye model,[25] in which a maximum in the out-of-phase component χ_M'' of the complex susceptibility is observed when the relaxation time τ equals $(2\pi\nu)^{-1}$. The frequency dependence of χ_M'' at constant temperature was here fitted using equation (1):

$$\chi_M''(\omega) = (\chi_T - \chi_S)[(\omega\tau)^{1-\alpha}\cos(\alpha\pi/2)]/[1 + 2(\omega\tau)^{1-\alpha}\sin(\alpha\pi/2) + (\omega\tau)^{2-2\alpha}] \quad (1)$$

where $\omega = 2\pi\nu$, χ_T and χ_S are the isothermal and adiabatic susceptibilities, *i.e.*, the susceptibilities observed in the two limiting cases $\nu \to 0$ and $\nu \to \infty$, respectively, and α is a parameter which accounts for a distribution of relaxation times.

Results and Discussion

The selectivity properties of the heterotopic bipyMO ligand in coordinating two different metal ions have been exploited to connect in an ordered chain 4*f* and 3*d* ions. In a previous work[26] we observed that the preparations of the lanthanide coordination polymers based on 4,4'-bipyridine (bipy) as divergent connector, $[Ln(\beta\text{-dik})_3bipy{\cdot}C_7H_8]_n$ (Ln = Eu, β-dik = dbm, tta, hfac; Ln = Tb; β-dik = dbm; Hdbm = dibenzoylmethane, Htta = thenoyltrifluoroacetone, Hhfac: hexafluoroacetylacetone), were easily performed in mild conditions and high yields starting from the anhydrous lanthanide β-diketonates provided that the absence of oxygen donor ligands was guaranteed. The bipyMO linker was expected to favour the alternate assembling of 3*d* and 4*f* ions used in 1:1 molar ratio also in the presence of water or other oxygen donor species. As a matter of fact, the treatment of a suspension of $[M(hfac)_2bipyMO]_n$ [9] (M = Zn, Cu or Co) in toluene with an equimolar amount of bipyMO induced a greater solubility of the starting CP, reasonably due to its fragmentation. The following addition of the lanthanide complex $[Ln(hfac)_3(H_2O)_2]$ (M = Zn, Cu and Ln = Eu or M = Co, Ln = Dy) produced the aggregation of the new 3*d*-4*f* heterometallic coordination polymers ($[Ln(hfac)_3M(hfac)_2(bipyMO)_2]_n$ (Ln = Eu, M = Zn, **1**; Ln = Eu, M = Cu, **2** and Ln = Dy, M = Co, **3**). The products were separated by filtration of the reaction mixture after

refluxing and cooling to room temperature. The derivatives can be recrystallized from methanol. Single crystals of **2** were selected for the determination of the crystalline and molecular structure by X-ray diffraction methods.– As hypothesized, in the mono-dimensional polymers the sequences −N═O−Ln−O═N−M−N═O− (N═O representing the bridging bipyMO) repeat regularly. Although expected, this outcome was not guaranteed, just for the lanthanide features, as discussed in the introduction, that make difficult to foresee their behaviour.

Compound **2** is made by linear chains of a coordination polymer where europium and copper regularly alternate. Europium atom shows eight-coordination in the shape of a square antiprism, while copper shows a six-coordination in the shape of an octahedron. The bipyridine monoxide spacer binds the lanthanide by the oxygen and the *d*-transition metal by the nitrogen, as shown in Figure 1. The coordination is completed by a number of bidentate hfac ligands which show some rotational disorder in the terminal CF_3 groups. The *d*-transition metals are placed on inversion centres and the metal ions along the chains are almost perfectly aligned, the angle Cu1···Eu···Cu2 being 179.5°. As it can be seen in Table 1, the Eu–O bond distances within the coordination polyhedron lie in a narrow interval (±1.4%) around the mean value 2.391 Å. Instead, the Cu–O distances within the coordination octahedra are more dispersed, especially in the case of Cu2, where the distances of two oxygen atoms of the same hfac from the metal differ by about 10 %. Such a marked difference may be due to the Jahn-Teller effect.

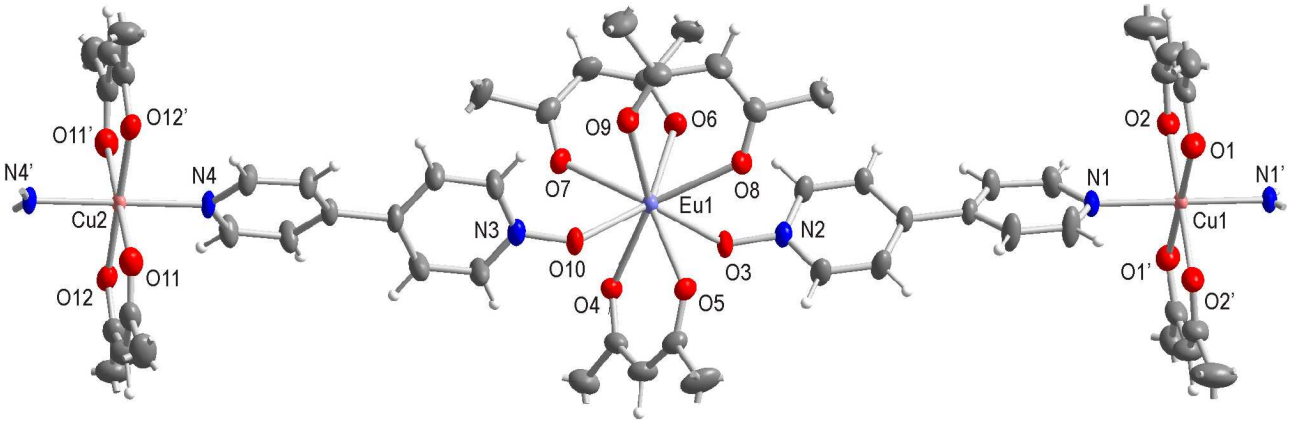

Figure 1. Molecular structure of the coordination polymer $[Eu(hfac)_3Cu(hfac)_2(bipyMO)_2]_n$. Disordered fluorine atoms of hfac ligands have been omitted for clarity.

Table 2. Bond distances (Å) around the metals.

Eu(1)–O(3)	**2.365(4)**	**Cu(1)–N(1)**	**2.053(4)**
Eu(1)–O(4)	**2.406(3)**	**Cu(1)–O(1)**	**2.253(5)**
Eu(1)–O(5)	**2.408(4)**	**Cu(1)–O(2)**	**2.030(4)**
Eu(1)–O(6)	**2.423(4)**	**Cu(2)–N(4)**	**2.043(4)**
Eu(1)–O(7)	**2.412(4)**	**Cu(2)–O(11)**	**2.164(5)**
Eu(1)–O(8)	**2.397(4)**	**Cu(2)–O(12)**	**2.080(5)**
Eu(1)–O(9)	**2.386(4)**		
Eu(1)–O(10)	**2.360(4)**		

In the crystal the polymer chains are all parallel running approximately in the [1 $\overline{10}$ 12] direction. Figure 2 shows two projections of one of these layers. As it can be seen in figure, along the chains, bulky sections, represented by the metals with their coordination spheres, alternate to slimmer ones, represented by the spacers. In the maximum density layers the staggered disposition of the chains allows them to approach at about 5.39 Å. So, the metals that in a single chain are rather far from each other (Eu1···Cu1 = 12.30 Å and Eu1···Cu2 = 12.29 Å) are closer among different chains. As it appears in Figure 2, each europium has two europium atoms at 7.41 and 7.49 Å, respectively, from opposite sides and in a very similar way each *d*-metal has two *d*-metal atoms at 7.45 Å from opposite sides. The shortest inter-chain Eu···Cu distances are 8.92 and 8.97 Å, respectively.

A

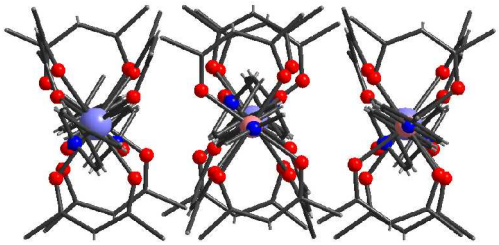

B

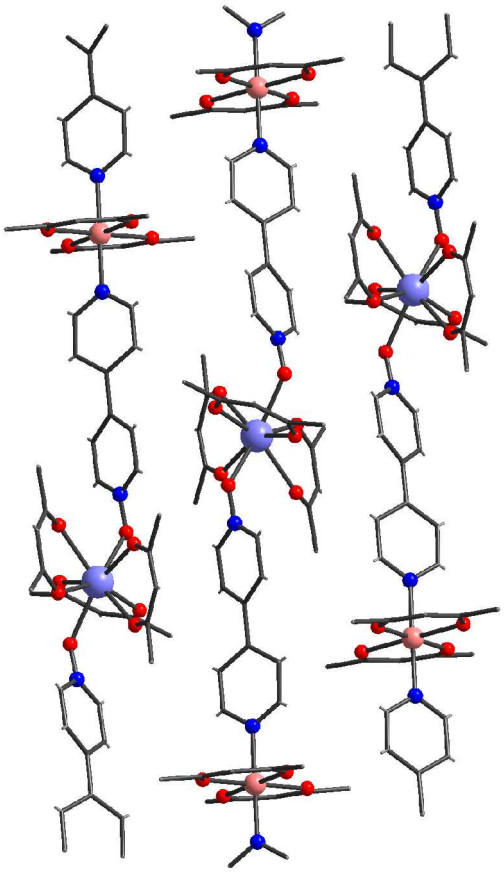

Figure 2. Views parallel (A) and normal (B) to the layer of maximum density.

Powder X-ray diffraction patterns carried out on the microcrystalline raw products pointed out that every species (**1**, **2**, **3**) was formed by a single crystalline phase, corresponding to the one determined by the single crystal diffraction experiments (Figure 3).

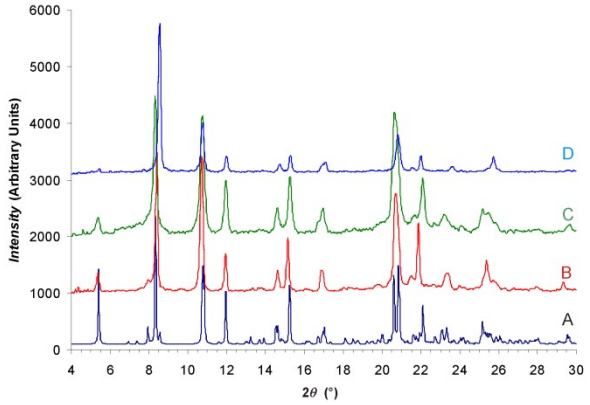

Figure 3. Comparison among the calculated X-ray diffraction pattern of **2** ($[Eu(hfac)_3Cu(hfac)_2(bipyMO)_2]_n$, A) and the experimental ones of **1** (B); **2** (C) and **3** (D).

Photoluminescence studies

Spectroscopic characterization was carried out at room temperature on microcrystalline powder samples. The photoluminescence excitation spectra (PLE, Figure 4a) of the 4*f*-3*d* coordination polymers are dominated by a broad band centred at ≈ 350 nm attributed to ligands-centred transitions (LCTs). The sensitized emission of Eu^{3+} is achieved thanks to the absorption properties of the β-diketonate and bipyMO ligands, according to the following steps: (i) absorption of light, (ii) intersystem crossing from the singlet to the triplet level, (iii) energy transfer from the chromophore to the lanthanide cation.[27] PLE indicates that europium emission can be excited in a wide wavelength range, from UV to visible (≈ 450 nm). Moreover, the only observable contribution of f-f transitions is due to $^7F_{0,1} \rightarrow {}^5D_2$ at 464 nm, whose intensity is small if compared to those of LCTs. The solid state absorption spectra of bipyMO and $[Zn(hfac)_2(bipyMO)]_n$, reported in the inset of Figure 4a, overlap with PLE confirming the role of the coordination polymer backbone in the sensitization of Eu^{3+} emission.

The photoluminescence spectra of **1** (Figure 4b) is characterized by the presence of a strong hypersensitive $^5D_0 \rightarrow {}^7F_2$ transition whose intensity is one order of magnitude larger than for $^5D_0 \rightarrow {}^7F_J$ J = 1, 3 and 4 Eu^{3+} emissions. The emission spectra recorded at different excitation wavelengths (between 290 nm and 470 nm) did not show any significant shape change.

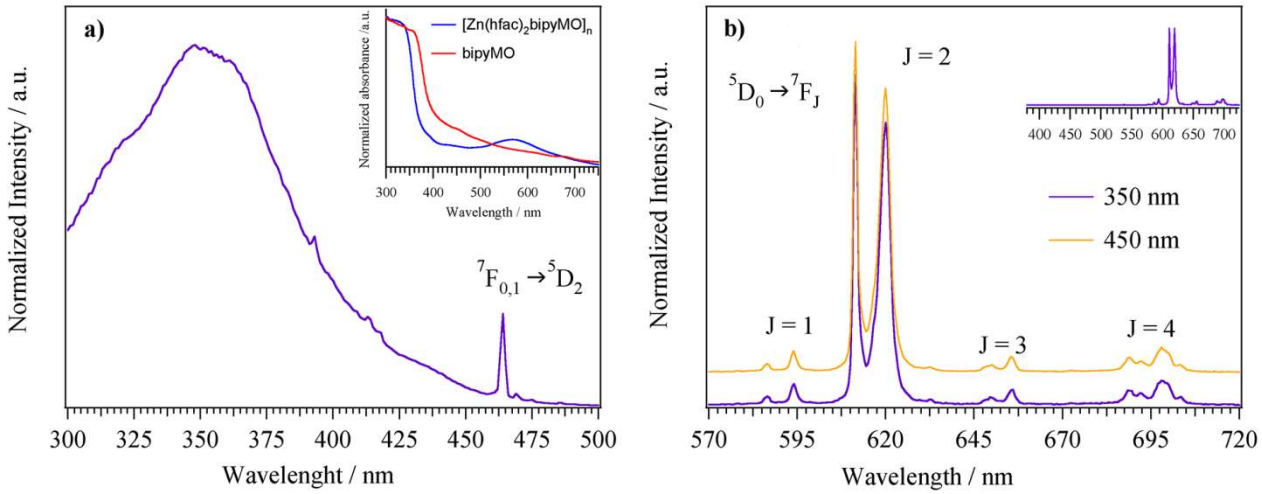

Figure 4. a) excitation spectrum of **1** monitored at 612 nm; inset: absorption spectra of bipyMO and $[Zn(hfac)_2(bipyMO)]_n$. **b)** emission spectrum of **1** excited at 350 and 450 nm. The extended emission spectrum (400 - 750 nm, λ_{exc} = 350 nm) of **1**, displayed in the inset, clearly shows the absence of any emission but those of europium.

Eu^{3+}-Zn^{2+} coordination polymers have very good emission performances with an absolute emission quantum yield (PLQY) of 0.24 which compares well with other Eu^{3+}-containing homo-metallic coordination polymers[28] and Zn-Eu 3D metal-organic frameworks[29].

At variance with **1,** derivative **2**, containing europium and copper, shows very weak emission (Figure S1). $[Cu(hfac)_2(bipyMO)]$ moieties present a strong absorption from 550 nm to near IR that overlaps with Eu^{3+} emission thus acting as an internal filter.

Magnetic properties of compound 3

The temperature dependence of the product of the molar magnetic susceptibility with temperature, $\chi_M T$, is displayed in Figure 5.

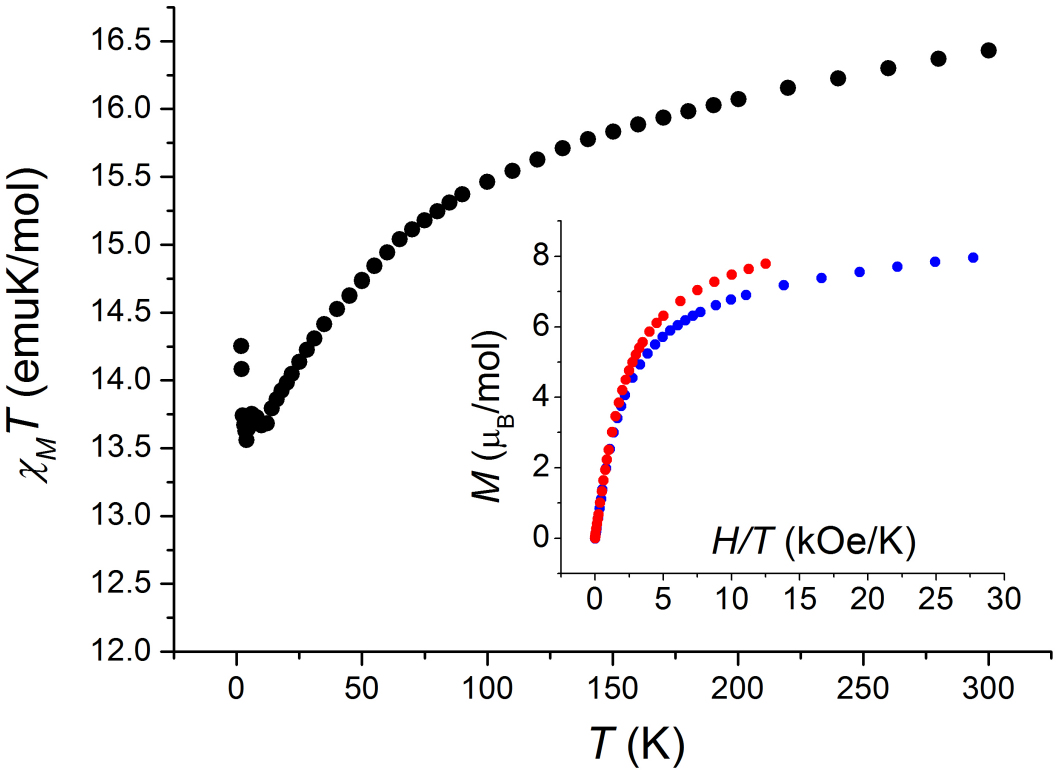

Figure 5. Temperature dependence of the $\chi_M T$ product for a pelletized sample of **3**. Inset: H/T dependence of isothermal magnetization taken at 1.8 K (blue circles) and 4.0 K (red circles).

The room temperature value of the $\chi_M T$ product, 16.4 emuK/mol, is above what expected for uncoupled Dy(III) ion (with an expected $\chi_M T$ value of 14.17 emuK/mol) and an octahedral high-spin Co(II) ion (with a spin-only expected $\chi_M T$ value of 1.875 emuK/mol) indicating the presence of an unquenched orbital contribution to the magnetic susceptibility of **3**, likely arising from the octahedral high-spin Co(II) ion. On cooling, the $\chi_M T$ value drops and reaches 13.6 emuK/mol at 2.1 K, as expected due to the depopulation of the crystal field Stark sublevels of the Dy(III) fundamental multiplet as well as the presence of orbital contribution of the Co(II) ions.[10] Below this temperature, the $\chi_M T$ product increases again to reach 14.3 emuK/mol at 1.8 K, suggesting the onset of ferromagnetic interactions in the solid state in the lowest temperature range. The non-overlapping nature of the isothermal molar magnetizations reveal the presence of magnetic anisotropy at low temperature. Absence of saturation of the magnetic moment at the highest field of 5 T suggests the presence of low-lying excited states, which may be responsible for the fast relaxation of the magnetization without a static applied field (*vide infra*).

The dynamics of the magnetization of **3** have been assessed by means of ac magnetic susceptibility analysis as a function of temperature, frequency and static field applied. In zero external field, the in-phase χ'_M and out-of-phase χ''_M susceptibilities showed a dependence on the measurement frequency below 5 K, but no χ''_M peaks were detected (Figure S2), suggesting that the magnetization dynamics is too fast to be characterized with our experimental setup. When a 0.1 T magnetic field was applied, however, a series of frequency dependent peaks appeared in the χ''_M versus T plot, as reported in Figure 6a, signalling the onset of slow relaxation of the magnetization of **3**. The fitting procedure of the frequency dependence of isothermal χ''_M profiles with a generalized Debye model, displayed in Figure S3, allowed the extraction of the temperature dependence of the characteristic magnetic relaxation time τ. The temperature dependence of τ is displayed in Figure 6b as an Arrhenius plot (ln τ versus T^{-1}). It can be seen that the plot is not linear, suggesting that the relaxation does not involve a simple thermally activated magnetization reversal over an anisotropic energy barrier.[30] The temperature dependence of the χ''_M peaks as well as the thermal evolution of the α parameter, which moves from 0.39 at 1.9 K to 0.26 at 2.8 K, rules out the presence of spin-glass behaviour of **3**.[31]

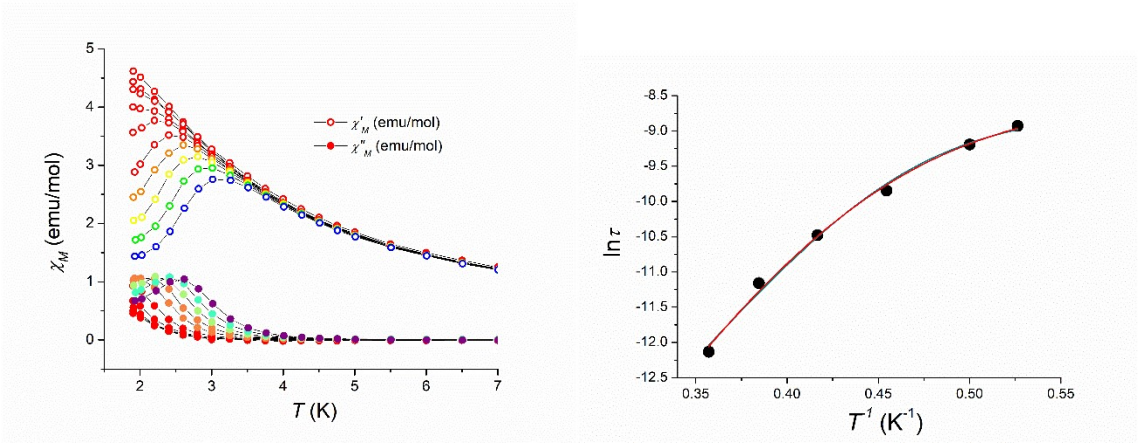

Figure 6. a) Temperature dependence of the in-phase χ_M' (empty circles) and out-of-phase χ_M'' (full circles) magnetic susceptibilities of **3**, measured in a static field of 0.1 T for ten logarithmically spaced frequencies spanning the 10 – 10^4 Hz frequency range. b) Arrhenius plot of the temperature dependence of the relaxation time of the magnetization τ for **3** in a 0.1 T static field, obtained from a best-fitting procedure of the isothermal $\chi_M''(\nu)$, as described in the Experimental Section. The lines represent the best fits obtained with the two models discussed in the text (green line: Raman + direct model, red line: Orbach + direct model).

In order to reproduce the $\tau(T)$ dependence, a relaxation model including different mechanisms was used:[10]

$$\frac{1}{\tau} = \frac{1}{\tau_0} e^{-\frac{U_{eff}}{kT}} + CT^n + AT$$

In this equation, the first term describes a classical, thermally activated overcome of an effective potential barrier U_{eff} by means of resonant spin-phonon coupling (Orbach process), the second term represents the magnetic relaxation by crossing through a virtual excited state (Raman process) and the last one pictures the direct phonon-induced relaxation. Due to the absence of peaks in the $\chi_M''(\nu)$ plot without a static field applied, no tunnelling mechanism of the magnetization was taken into account. The results of the best fitting procedure based in the model above exposed are reported as full lines in Figure 6b. Two different relaxation mechanisms yielded fitting functions of similar goodness. The first one (red line, $R^2 = 0{,}994$) mixed direct and Raman mechanisms, giving C = 1(1) $K^{-n}s^{-1}$, n = 11(1), A = 3.3(4)·10^3 $K^{-1}s^{-1}$, the second one employed a mixed direct and Orbach one (green line, $R^2 = 0{,}991$), yielding τ_0 = 1(1) ·10^{-10} s, U_{eff} = 21(1)cm^{-1}, A = 3.8(4)·10^3 $K^{-1}s^{-1}$. In both cases, the presence of the direct mechanism reproduced the low temperature region of the plot, while the other described the higher temperature region. When compared with the results obtained for a radical bridged DyCo heteronuclear chain,[3c] the experimental barrier found in this work appears about eight times higher, suggesting that the presence of antiferromagnetic interactions may provide additional relaxation pathways to these heterometallic systems.

Conclusions

We describe in this paper the first example of monodimensional heterometallic coordination polymers assembled with bipyMO as bridging ligand between 4*f* and 3*d* metal ions, and based on the selection power exerted by the heterotopic connector. In the three CPs, $[Ln(hfac)_3M(hfac)_2(bipyMO)_2]_n$ (Ln=Eu, M=Zn, Cu; Ln=Dy, M=Co), lanthanide and *d* metal ions regularly alternate. In the nodes, $Ln(hfac)_3$ and $M(hfac)_2$, the metal centres complete their coordination spheres with two oxygen- and two nitrogen-coordinated bipyMO connectors, respectively. Their self-assembling process was driven by the different affinity of the two different metal ions for nitrogen and oxygen donor ligands. X-ray diffraction studies showed that the three derivatives are isotypic. Photoluminescence studies evidenced a bright red emission for **1** with absolute PL quantum yield of 0.24. BipyMO and $[Zn(hfac)_3bipyMO]_n$ contribute to sensitize europium emissions that can be excited in a wide wavelength range, from UV to visible, up to ≈ 450 nm. The contribution of the 3*d* metal to the emission properties cannot be clearly distinguished.

This aspect will be studied in more detail in future works. From the magnetic point of view, **3** showed the presence of a very weak ferromagnetic interaction in the solid state as well as a slow relaxation of the magnetization when immersed in a 0.1 T static magnetic field. The temperature dependence of the relaxation times could be equally fitted with two different models, the first one including a mixed Raman-direct process and a second one featuring a mixed Orbach-direct mechanism, yielding an effective barrier for the thermal relaxation of 21(1) cm^{-1}. Further studies on this topic are ongoing in view of the possibility to prepare a wide variety of similar derivatives whose properties (magnetic, optic, catalytic) can be tuned by the appropriate choice of the 3*d*-4f metal ion couple.

Acknowledgements

The authors thank the Università di Pisa (Fondi di Ateneo 2014 and 2015 and PRA_2016_50 Materiali Funzionali, Progetti di Ricerca di Ateneo), Ministero Istruzione Università e Ricerca, MIUR (PRIN 2015 **20154X9ATP** Progetti di Ricerca di Interesse Nazionale) and the Brazilian Conselho Nacional de Desenvolvimento Científico e Tecnológico (Projeto Universal 2016) for financial support.

Notes and References

1 (*a*) M. Sakamoto, K. Manseki and H. Ōkawa, *Cood. Chem. Rev.*, 2001, **219-221**, 379; (b) Y. J. Cui, Y. F. Yue, G. D. Qian and B. L. Chen, *Chem. Rev*., 2012, **112**, 1126; (c) L. Sorace, C. Benelli and D. Gatteschi, *Chem. Soc. Rev.* 2011, **40**, 3092.

2 (a) O. Guillou, P. Bergerat, O. Kahn, E. Bakalbassis, K. Boubekeur, P. Batail and M. Guillot, *Inorg. Chem*. 1992, **31**, 110; (b) C. L. Cahill, D. T. de Lill and M. Frisch, *CrystEngComm*, 2007, **9**, 15; (c) M. Andruh, J.-P. Costes, C. Diaz and S. Gao, *Inorg. Chem.*, 2009; **48**, 334; (d) K. Liu, W. Shi and P. Cheng, *Coord. Chem. Rev.,* 2015, **289-290**, 74.

3 (a) M. Yang, J. Sun, J. Guo, G. Sun and L. Li, *CrystEngComm.,* 2016, **18**, 9345; (b) B. Yao, Z. Guo, X. Zhang, Y. Ma, Z. Yang, Q. Wang, L. Li and Peng Cheng, *Cryst.Growth Des.,* 2017, **17**, 95; (c) X. Wang, H. Li, J. Sun, M. Yang, C. Li and L. Li, *New J.Chem.,* 2017, **41**, 2973; (d) M. Zhu, C. Li, X. Wang, L. Li and J.-P. Sutter, *Inorg.Chem.,* 2016, **55,** 2676.

4 C. Wang, S.-Y. Lin, W. Shi, P. Cheng and J. Tang, *Dalton Trans.,* 2015, **44**, 5364.

5 (a) K. Biradha, M. Sarkar and L. Rajput, *Chem. Commun.*, 2006, **41**, 4169; (b) H. W. Roesky and M. Andruh, *Coord. Chem. Rev.*, 2003, **236**, 91.

6 (a) D. Long, A. J. Blake, N. R. Champness, C. Wilson and M. Schröder, *Chem. Eur. J.*, 2002, **8**, 2026; (b) W. Zhu and Y. He, *J. Coord. Chem.,* 2002, **55**, 251; (c) S. Ma, W. Zhu, G. Huang, D. Yuan and X. Yan, *J. Mol. Struct*., 2003, **646**, 89.

7 (a) O. Toma, N. Mercier, M. Bouilland and M. Allain, *CrystEngComm*, 2012, **14**, 7844; (b) A. A. Dar, G. A. Bhat and R. Murugavel, *Inorg. Chem.*, 2016, **55**, 5180; (c) O. Toma, M. Allain, F. Meinardi, A. Forni, C. Botta and N. Mercier, *Angew. Chem. Int. Ed.*, 2016, **55**, 7998; (d) O. Toma, N. Mercier, M. Allain, F. Meinardi and C. Botta, *Eur. J. Inorg. Chem.*, 2017, 844.

8 (a) D. J. Hoffart, N. C. Habermehl and S. J. Loeb, *Dalton Trans.*, 2007, 2870; (b) O. Toma, N. Mercier, M. Allain and C. Botta, *CrystEngComm*, 2013, **15**, 8565; (c) V. N. Vukotic and S. J. Loeb, *Supramolecular Chemistry*, 2016, **28**, 151.

9 D. Belli Dell'Amico, S. Ciattini, L. Fioravanti, L. Labella, F. Marchetti, C. A. Mattei, and S. Samaritani, *Polyhedron*, 2018, **139**, 107.
10 N. N. Greenwood, A. Earnshaw, *Chemistry of the Elements*, second Edition, 1997, reprinted 2008, Elsevier, Amsterdam.
11 R. J. Carlin, *Magnetochemistry*, Springer, Berlin, 1986.
12 N. Ishikawa, M. Sugita, T. Ishikawa, S.-Y. Koshihara and Y. Kaizu, *J. Am. Chem. Soc.*, 2003, **125**, 8694.
13 T. Grancha, J. Ferrando-Soria, M. Castellano, M. Julve, J. Pasan, D. Armentano and E. Pardo, *Chem. Commun*., 2014, **50**, 7569.
14 (a) L.-F. Zou, L. Zhao, Y.-N. Guo, G.-M. Yu, Y. Guo, J. Tang and Y.-H. Li, *Chem. Commun*., 2011, **47**, 8659; (b) X. Yang, R. A. Jones and S. Huang, *Coord. Chem. Rev.*, 2014, **273-274**, 63; (c) J. Goura, A. Chakraborty, J. P. S. Walsh, F. Tuna and V. Chandrasekhar, *Cryst. Growth Des.*, 2015, **15**, 3157.
15 (a) K. Bernot, L. Bogani, A. Caneschi, D. Gatteschi and R. Sessoli, *J. Am. Chem. Soc*., 2006, **128**, 7947; (b) G. Poneti, K. Bernot, L. Bogani, A. Caneschi, R. Sessoli, W. Wernsdorfer and D. Gatteschi, *Chem. Commun*., 2007, **18**, 1807.
16 (a) C. Benelli and D. Gatteschi. In *Introduction to Molecular Magnetism: from Transition Metals to Lanthanides*, Chp. 14 *SMM with Lanthanides*, Wiley-VCH Verlag, 2015, 239, ISBN-10: 978-3527335404. (b) R. A. Layfield and M. Murugesu. In *Lanthanides and Actinides in Molecular Magnetism*. Wiley-VCH, 2016. ISBN: 978-3527335268. (c) K. Liu, X. Zhang, X. Meng, W. Shi, P. Cheng and A. K. Powell, *Chem. Soc. Rev.,* 2016, **45**, 2423.; (d) D. N. Woodruff, R. E. P. Winpenny and R. A. Layfield, *Chem. Rev*., 2013, **113**, 5110.
17 W. Wernsdorfer, N. Aliaga-Alcalde, D. N. Hendrickson and G. Christou, *Nature*, 2002, **416**, 406.
18 S. M. T. Abtab, M. C. Majee, M. Maity, J. Titiš, R. Boča and M. Chaudhury, *Inorg. Chem*., 2014, **53,** 1295.
19 S.J. Lyle, A.D. Witts, *Inorg. Chim. Acta*, 1971, **5**, 481.
20 Bruker (2008). APEX2 (Version 2008.1-0). Bruker AXS Inc., Madison, Wisconsin, USA
21 G. M. Sheldrick, (1996). SADABS. Program for Empirical Absorption Correction. University of Gottingen, Germany.
22 G. M. Sheldrick, *Acta Crystallogr., Sect. A: Found. Crystallogr.*, 2008, **64**, 112.
23 L. J. Farrugia, *J. Appl. Cryst.*, 1999, **32**, 837.
24 G. A. Bain and J. F. J. Berry, *Chem. Educ*., 2008, **85**, 532.
25 (a) K. S. Cole and R. H. Cole, *J. Chem. Phys.*, 1941, **9**, 341; (b) C. Dekker, A. F. M. Arts, H. W. Dewijn, A. J. Vanduyneveldt and J. A. Mydosh, *Phys. Rev. B*, 1989, **40**, 11243.
26 L. Armelao, D. Belli Dell'Amico, L. Bellucci, G. Bottaro, L. Labella, F. Marchetti and S. Samaritani, *Polyhedron*, 2016, **119**, 371.
27 J. C. G. Bünzli, *Coord. Chem. Rev.,* 2015, **293-294**, 19.
28 (a) S.V. Eliseeva, D.N. Pleshkov, K.A. Lyssenko, L.S. Lepney, J.G. Bunzli and N.P.J Kuzmina, *Inorg.Chem*., 2010, **49**, 9300; (b) K. Miyata, T. Ohba, A. Kobayashi, M. Kato, T. Nakanishi, K. Fushimi and Y. Hasegawa. *Chem.Plus.Chem,* 2012*,* **77***,* 277.
29 C. B. Liu, R. A. S. Ferreira, F. A. Almeida Paz, A. Cadiau, L. D. Carlos, L. S. Fu, J. Rocha and F.-N. Shi *Chem. Commun.*, 2012, **48**, 7964.
30 D. Gatteschi, R. Sessoli and J. Villain, *Molecular Nanomagnets*; Oxford University Press: Oxford, U.K., 2006.
31 J. A. Mydosh, *Spin Glasses: An Experimental Introduction*; Taylor & Francis, London, 1993.